J Mol Model (2008) 14:427–434
DOI 10.1007/s00894-008-0291-2

ORIGINAL PAPER

Molecular modeling and dynamics studies of cytidylate kinase from *Mycobacterium tuberculosis* H37Rv

Rafael Andrade Caceres · Luís Fernando Saraiva Macedo Timmers · Ana Luiza Vivan · Cristopher Zandoná Schneider · Luiz Augusto Basso · Walter Filgueira De Azevedo Jr. · Diogenes Santiago Santos

Received: 10 December 2007 / Accepted: 12 February 2008 / Published online: 15 March 2008

Abstract Bacterial cytidylate kinase or cytidine monophosphate kinase (CMP kinase) catalyses the phosphoryl transfer from ATP to CMP and dCMP, resulting in the formation nucleoside diphosphates. In eukaryotes, CMP/UMP kinase catalyses the conversion of UMP and CMP to, respectively, UDP and CDP with high efficiency. This work describes for the first time a model of bacterial cytidylate kinase or cytidine monophosphate kinase (CMP kinase) from mycobacterium tuberculosis (MtCMPK). We modeled MtPCMPK in apo form and in complex with cytidine 5′-monophosphate (CMP) to try to determine the structural basis for specificity. Comparative analysis of the model of MtCMPK allowed identification of structural features responsible for ligand affinities. Analysis of the molecular dynamics simulations of these two systems indicates the structural features responsible for the stability of the structure, and may help in the identification of new inhibitors for this enzyme.

Keywords Cytidine 5′-monophosphate · Enzyme substrate specificity · Molecular dynamics · Molecular modeling · Mycobacterium tuberculosis

Abbreviations

TB	tuberculosis
CMPK	cytidine monophosphate kinase
MDR-TB	multidrug resistant TB
MD	molecular dynamic

Introduction

Tuberculosis (TB) remains one of the deadliest diseases worldwide. World Health Organization estimates that one third of the population is infected with *Mycobacterium tuberculosis*, the causative agent of TB [1]. It has been estimated that there are approximately 8 million new cases of TB every year and 2 million deaths occur each year [2]. The reemergence of TB is due to the high incidence of AIDS, the proliferation of drug-resistant strains and the decline in health care structures and national surveillance. It has been pointed out that the emergence and spread of multi-drug resistant strains of *M. tuberculosis* (MDR-TB), defined as resistant to at least isoniazid and rifampicin, could threaten global TB control [3]. More recently, a survey of the frequency and distribution of extensively drug-resistant (XDR) TB cases showed that during 2000–2004, of 17,690 TB isolates, 20% were MDR and 2% were XDR [4]. XDR-TB is defined by the World Health

R. A. Caceres
Programa de Pós Graduação em Biologia Celular e Molecular, Pontifícia Universidade Católica do Rio Grande do Sul, Porto Alegre, RS, Brazil

R. A. Caceres · L. F. S. Macedo Timmers · A. L. Vivan · W. F. De Azevedo Jr. (✉)
Faculdade de Biociências, Laboratório de Bioquímica Estrutural, Pontifícia Universidade Católica do Rio Grande do Sul, Porto Alegre, RS, Brazil
e-mail: walter.junior@pucrs.br

C. Z. Schneider · L. A. Basso · D. S. Santos
Centro de Pesquisas em Biologia Molecular e Funcional, Instituto de Pesquisas Biomédicas, Pontifícia Universidade Católica do Rio Grande do Sul, Porto Alegre, RS, Brazil

D. S. Santos
e-mail: diogenes@pucrs.br

Organization as resistance to at least rifampin and isoniazid plus resistance to the fluoroquinolones and to at least one of the injectable drugs capreomycin, kanamycin and amikacin [5]. XDR-TB has a wide geographic distribution [6] and high fatality rate [7]. The emergence of XDR-TB worldwide raises the bleak prospect of virtually untreatable TB. There is thus an urgent need for the development of new chemotherapeutic agents to treat TB.

CMP kinases belong to a family called nucleoside monophosphate kinases (NMK), which are key enzymes in the metabolism of nucleotides [8]. Substrate specificity studies on recombinant human UMP/CMP kinase (pyrimidine nucleoside monophosphate kinase) has shown that UMP and CMP are far better substrates than dCMP [9]. Bacterial cytidylate kinase or cytidine monophosphate kinase (CMP kinase) catalyses the phosphoryl transfer from ATP to CMP and dCMP, resulting in the formation of nucleoside diphosphates. CMP kinase has been shown to be essential for bacterial growth in *Streptococcus pneumoniae* [10]. The *Staphylococcus aureus* CMP kinase crystal structure has recently been resolved [11]. The crystal structure of *Escherichia coli* CMP kinase resembles those of other NMP kinases sharing common features such as a central five-stranded β-sheet connected by α-helices, a fingerprint sequence of Glu-x-x-Gly-x-Gly-Lys (P-loop), and an anion hole in the central cavity for substrate binding [12]. However, *E. coli* CMP kinase contains an insertion of 40 residues and a short LID domain, differing from other NMP kinases [12]. These differences could allow the rational design of drugs specific for CMP kinase of pathogenic bacteria, such as *M. tuberculosis*. However, no report has yet described the three-dimensional structure of *M. tuberculosis* CMP kinase. In the present work we modeled the structure of CMPK from *M. tuberculosis* (*Mt*CMPK). It was analyzed the structure of *Mt*CMPK in complex with cytidine-5′-monophosphate (CMP) to identify the structural basis for the substrate interactions in the binding site and to predict the enzyme substrate specificity. The structural features and the structural stability were assessed by molecular dynamic (MD) simulation.

Materials and methods

Molecular modeling

Homology modeling is usually the method of choice when there is a clear relationship of homology between the sequences of a target protein and at least one experimentally determined three-dimensional structure. This computational technique is based on the assumption that tertiary structures of two proteins will be similar if their sequences were related, and it is the approach most likely to give accurate results [13].

For modeling of the *Mt*CMPK we used restrained-based modeling implemented in the program MODELLER 9v1 [14]. This program is an automated approach to comparative modeling by satisfaction of spatial restrains [15]. The modeling procedure begins with alignment of the sequence to be modeled (target) with related known three-dimensional structures (templates). This alignment is usually the input to the program and the output is a three-dimensional model for the target sequence containing all main-chain and side-chain non-hydrogen atoms [16].

The high degree of primary sequence identity between *Mt*CMPK (target) and of *E.coli* indicates that these crystallography structures are good models to be used as templates for *Mt*CMPK enzyme (target). The alignment of the *Mt*CMPK (target) and *E. coli* CMPK is shown in Fig. 1 [17].

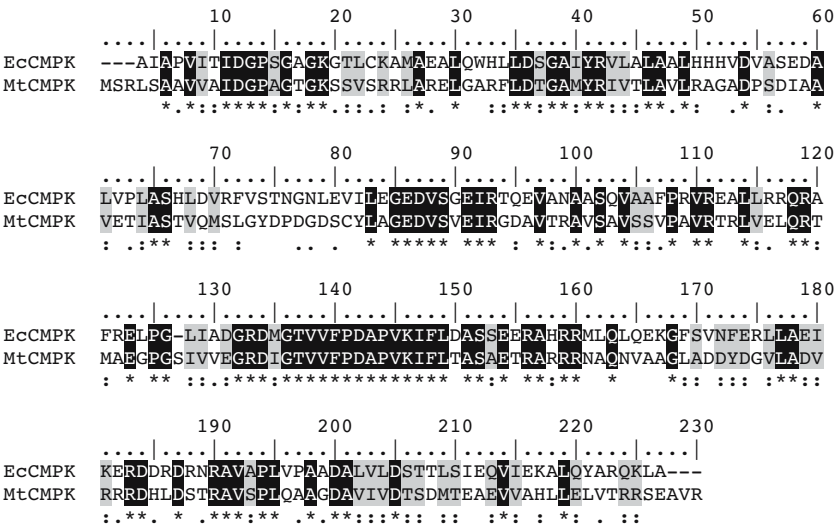

Fig. 1 Sequence alignment for *Ec*CMPK and *Mt*CMPK The sequence identity between *Ec*CMPK and *Mt*CMPK is ~40%. The alignment was performed using ClustalW and edited with BioEdit [17]

A total of 1000 models were generated for each binary complex and the final models were selected based on the MODELLER [14] objective function.

Evaluation of binding affinity

Analysis of the interaction between a ligand and a protein target is still a scientific endeavor. The affinity and specificity between a ligand and its protein target depend on directional hydrogen bonds and ionic interactions, as well as on shape complementarity of the contact surfaces of both partners [18]. We used the programs X-SCORE [19], SCORE [20] and PEARLS [21] to evaluate the binding affinity of the ligand against *E. coli CMPK* and *Mt*CMPK.

Analysis of the models

The overall stereochemical quality of the final models for each enzyme of the *Mt*CMPK was assessed by the program PROCHECK [22, 23] and the objective function supplied of the MODELLER [14].

Molecular dynamic simulations

MD simulations were performed with the GROMACS [24] package using the Gromos 96.1 (43A2) force field. The CMP topology was generated with the PRODRG program [25]. Accurate force fields are essential for reproducing the conformational and dynamic behavior of condensed-phase systems, the Gromos 96.1 force fields are well parameterized for proteins but the parameters for small molecules are still limited for simulations of more complicated biological systems. Accordingly, GAMESS was used for the atomic charges in the CMP molecule [26], which were submitted to single-point ab initio calculations at RHF 6-31G* level in order to obtain Löwdin derived charges. Manipulation of structures was performed with Swiss-PDBViewer v3.7 program [27]. The first system was composed by apoenzyme MtCMPK (system 1) and the second by MtCMPK enzyme, three sulphate ions and CMP ligand (system 2). The simulations of two systems were performed by a time period of 3 ns. Na^+ counter ions were added to both systems (six Na^+ ions on system 1 and 14 Na^+ ions on system 2) using Genion Program of the GROMACS simulation suite to neutralize the negative charge density of the systems.

Each structure was placed in the center of a truncated cubic box filled with simple point charge (SPC/E) water molecules [28], containing 14,993 water molecules for system 1 and 16,741 water molecules for system 2. The initial simulation cell dimensions were 44.78×47.23×49.38 Å for system 1 and 51.37×48.76×55.23 Å for system 2, and had the protein solvated by a layer of water molecules of at least 10 Å length in all directions in both systems. During the simulations, bonds lengths within the proteins were constrained by using LINCS algorithm [29]. The SETTLE algorithm was used to constrain the geometry of water molecules [30]. In the MD protocol, all hydrogen atoms, ions, and water molecules were first subjected to 1000 steps of energy minimization by steepest descent followed by 500 steps of conjugate gradient to remove close van der Waals contacts. The systems were then submitted to a short molecular dynamic with position restrains for a period of 20 ps and afterwards performed a full molecular dynamics without restrains. The temperature of the system was then increased from 50 to 300 K in 5 steps (50 to 100 K, 100 to 150 K, 150 to 200 K, 200 to 250 K, 250 to 300 K), and the velocities at each step were reassigned according to the Maxwell-Boltzmann distribution at that temperature and equilibrated for 10 ps except the last part of termalization phase that were for 40 ps. Energy minimization and MD were carried out under periodic boundary conditions. The simulation was computed in the NPT ensemble at 300 K with the Berendsen temperature coupling and constant pressure of 1 atm with isotropic molecule-based scaling [31]. The LINCS algorithm, with a 10^{-5} Å tolerance, was applied to fix all bonds containing a hydrogen atom, allowing the use of a time step of 2.0 fs in the integration of the equations of motion. No extra restraints were applied after the equilibration phase. The electrostatic interactions between nonligand atoms were evaluated by the particle-mesh Ewald method [32] with a charge grid spacing of ~ 1.0 Å and the charge grid was interpolated on a cubic grid with the direct sum tolerance set to 1.0×10^{-5}. The Lennard-Jones interactions were evaluated using a 9.0 Å atom-based cutoff [33].

All analyses were performed on the ensemble of system configurations extracted at 0.5-ps time intervals from the simulation and MD trajectory collection was initiated after 1 ns of dynamics to guarantee a completely equilibrated evolution. The MD simulation and results analysis were performed on a personal computer Intel Core 2 Duo E6300 - 1,86 GHz and 4 Gb RAM.

The convergences of the different simulations were analyzed in terms of the secondary structure, root mean-square deviation (RMSD) from the initial models structures, and root mean-square fluctuation (RMSF).

For the RMSFs were calculated relative to the last 2 ns averaged backbone structures, and all coordinate frames from the trajectories were first superimposed on the initial conformation to remove any effect of overall translation and rotation.

Results and discussion

Quality of the models

There is no crystallographic structure available for *Mt*CMPK, however the sequence identity (38.70%) be-

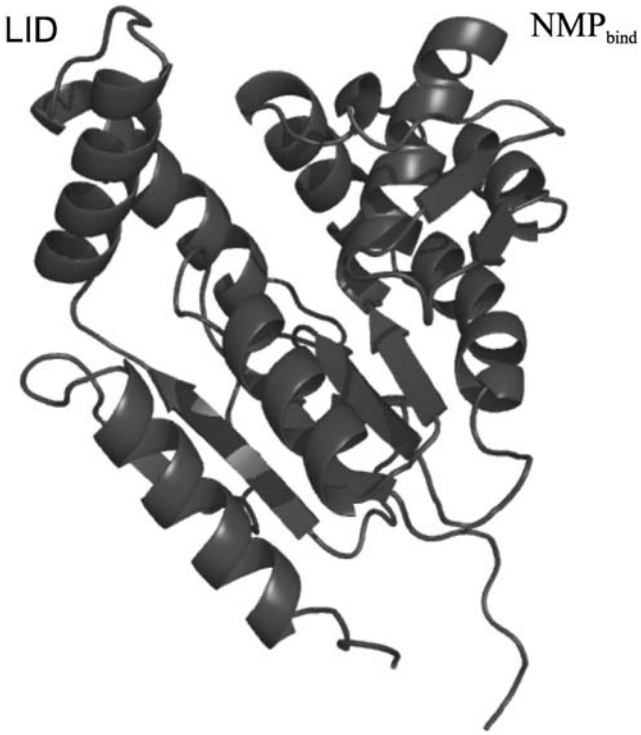

Fig. 2 Tertiary structure of the apoenzyme *Mt*CMPK. The structure is presented as a ribbon diagram. The structure contains ten alpha-helices surround by seven-stranded β-sheet. The image was generated using Pymol [22]

tween *Mt*CMPK and *E. coli* CMPK (PDB access code: 1KDO) sequences makes *E. coli* CMPK structure a good template for modeling of *Mt*CMPK. The atomic coordinates of crystallography structures of template were hence used as basic models for MtCMPK modeling. The atomic coordinates of all water molecules were removed from the templates.

The analysis of the Ramachandran diagram φ - ψ plots for the template (E. coli CMPK) was used to compare the overall stereochemical quality of the MtCMPK structure against those of the template solved by biocrystallography. The homology model has over 92.1% of the residues in the most favorable regions.

Overall description

The structural model of the *Mt*CMPK contains a seven beta-ribbon motif. The beta-ribbons are composed of residues 7–12, 33–37, 69–75, 78–84, 127–132, 145–150 and 202–206. Ten alpha - helices surround the beta - ribbon structure. The helical regions are composed of residues 19–30, 38–51, 58–66, 89–91, 95–105, 109–120, 134–138, 153–167, 173–189 and 211–225. Figure 2 shows a schematic drawing of the *Mt*CMPK structure (monomer). As described in the *M. tuberculosis* H37Rv genome annotation [34], the model of *Mt*CMPK consists of 230 amino acids with a predicted molecular mass of 24,177.29 Da and a theoretical pI value of 5.05. The *E. coli CMPK* consists of 223 amino acids with a predicted molecular mass of 24,746.34 Da and a theoretical pI value of 5.56. Analysis of both structures indicates the conservation of the residues that make intermolecular hydrogen bonds with cytidine-5′-monophosphate.

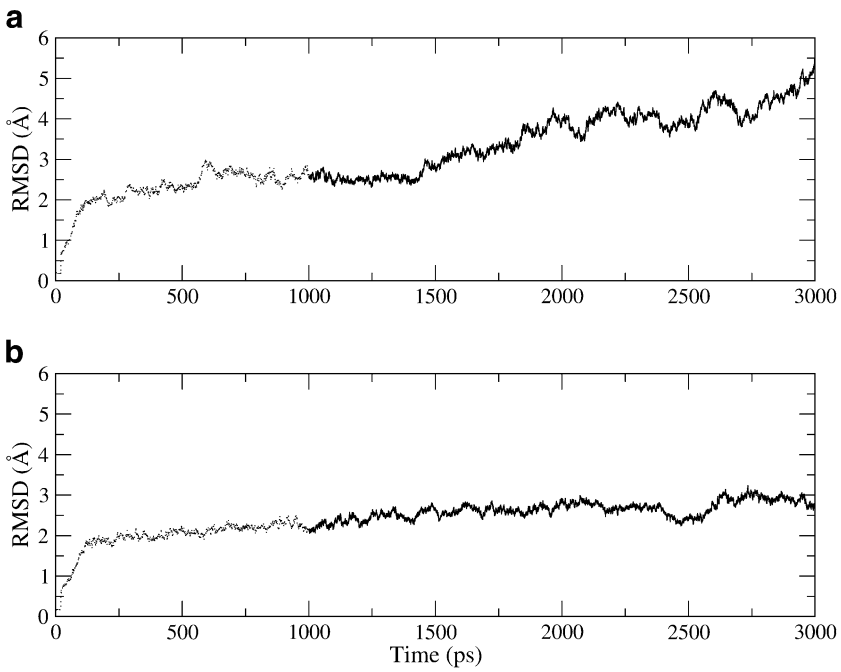

Fig. 3 Graphical representation of root-mean-square deviation (RMSD) of all Cα from starting structure of models as a function of time. The graphic **a** shows the RMSD of apoenzyme *Mt*CMPK, **b** graphic shows the RMSD of *Mt*CMPK-CMP complex. The dashed line gives the equilibration phase, the solid line shows the last 2 ns of calculation

Fig. 4 Superposition of the average during the last of 2000 snapshots with the initial minimized structure of *Mt*CMPK-CMP. The structures are presented as ribbon diagram. The average structure is colored light gray; the initial structure is colored dark gray

MD simulations

We performed molecular dynamics simulations of the *Mt*CMPK structure in the apo form (system 1) and the complex *Mt*CMPK:CMP (system 2) to elucidate the influence of CMP on the overall structure of the *Mt*CMPK. The root-mean square deviation (RMSD) of the positions for all backbone C-alpha atoms from their initial configuration as a function of simulation time for all systems were calculated and are shown in Fig. 3. Analysis of this figure indicates that the structure without ligand presents high RMSD when compared with the structure of the binary complex.

As shown in Fig. 3a system 1 presents an increase in RMSD values during overall MD simulation showing a relative stability between 250 and 1500 ps. On the other hand, system 2 after a rapid increase during the first 250 ps reaches a plateau of 2.6±0.2 Å value for RMSD of all C-alpha atoms. Figure 3b, suggests that that 2980 ps unrestrained simulation was sufficient for stabilizing a fully relaxed *Mt*CMPK-CMP model. Accordingly, the *Mt*CMPK-CMP binary complex structure appears to be more stable than the apo form of the enzyme.

Superposition of the average structure of system 2 with the initial model (Fig. 4) does not show major conformational changes from the initial model, which is consistent with the relatively low RMSD value. System 1 presents high RMSD values, however its secondary structure was kept (Fig. 5), and these high values are due to the flexibility of the apo form of *Mt*CMPK.

The flexibilities of the proteins were assessed by the RMSF values from MD of the trajectory which reflects the flexibility of each atom residue in a molecule (Fig. 6). The major backbone fluctuation occurs in the loop region and in the region surrounding the beta-alpha-beta fold, whereas regions with the low RMSF correspond exclusively to the rigid beta-alpha-beta fold. These results indicate the stability of our model structures.

LID domain

The *Mt*CMPK structure model as *E. coli* CMP kinase contains a short LID domain [12]. Shikimate Kinase from *M. tuberculosis* (*Mt*SK), a member of NMP kinase family,

Fig. 5 Superposition of the average during the last of 2000 snapshots with the initial minimized structure of aporenzyme *Mt*CMPK. The structures are presented as ribbon diagram. The average structure is colored light gray; the initial structure is colored dark gray

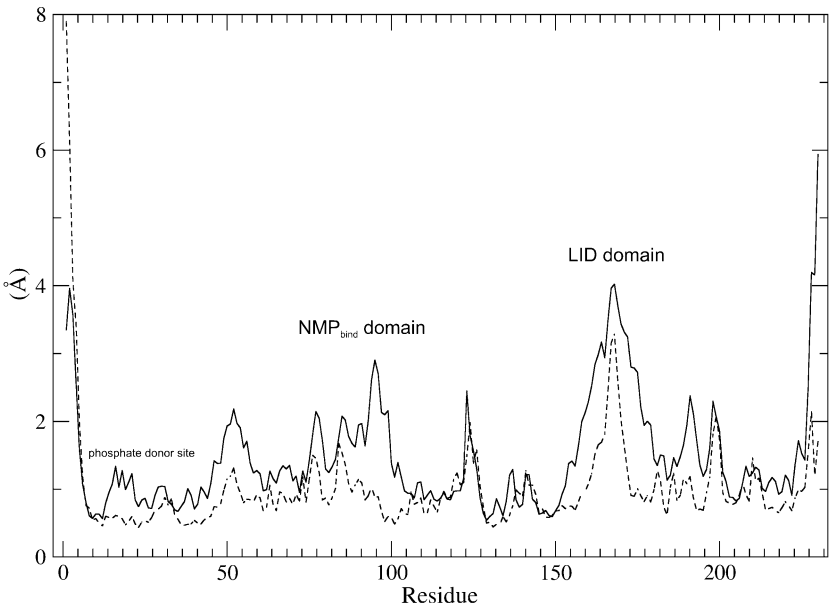

Fig. 6 Graphical representation of root-mean-square fluctuations (RMSF) of all Cα from starting structure of models as a function of time. The graphic shows the RMSF of apoenzyme *Mt*CMPK and of *Mt*CMPK-CMP complex. The average of the last 2 ns of calculation is given in the dashed line apoenzyme *Mt*CMPK and the solid line shows *Mt*CMPK-CMP complex

has three domains: the CORE, LID and NMP-binding domains. A comparison between the crystal structure of *Mt*SK structure in complex with MgADP and *Erwinia chrysanthemi* SK suggested a concerted conformational change of the LID and shikimate binding (SB) domains upon nucleotide binding [35, 36]. More recently, a comparison between the structures of *Mt*SK-MgADP-shikimate dead-end ternary complex and the MtSK-MgADP binary complex showed that the LID and SB domains undergo concerted movements toward each other [37], resulting in an additional closure of the enzyme active site. The RMSF values calculated for both systems described here suggest that a short LID domain in *Mt*CMPK may undergo conformational changes as observed for the structure of *Mt*SK (Fig. 6).

The LID of *Mt*CMPK corresponds to the Arg160-Asp174 domain. The large mobility of LID domain is consistent with the need for this region to undergo conformational changes upon substrate binding to shield the enzyme active site from water in order to avoid ATP hydrolysis [38]. In the LID domain the behavior differences between system 1 and system 2 is evident and the LID domain appears in a more open conformation in apoenzyme than in *Mt*CMPK-CMP (Fig. 7), demonstrating that the CMP induces a major stability of this region, as the substrate binding loop and is involved in substrate entrance and exit.

The NMP$_{bind}$ domain

The NMP$_{bind}$ domain has also been described as undergoing motions when it binds the phosphoryl acceptor substrate. The NMP$_{bind}$ domain of *Mt*CMPK corresponds to the segment Gly38-Glu123. As GMP kinases from yeast, the *Mt*CMPK has a two-stranded β sheet in the NMP$_{bind}$ domain [12], contrary to *Ec*CMPK that contains a three-

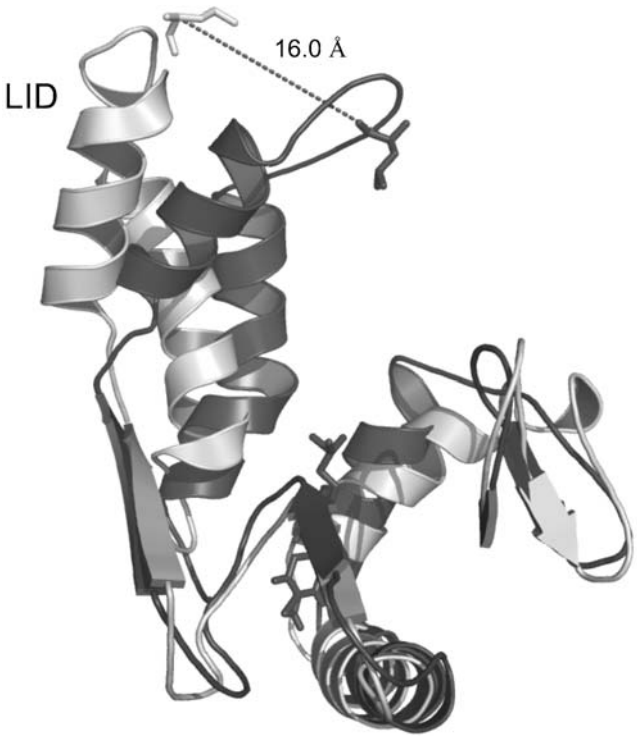

Fig. 7 Superposition of the apoenzyme *Mt*CMPK with the structure of *Mt*CMPK-CMP showing the LID domain, the distance of Leu169 (C-alpha) between both structures is shown. The structure of the apoenzyme *Mt*CMPK is colored light gray and *Mt*CMPK-CMP structure is colored dark gray

stranded antiparallel β sheet [11]. The RMSD for the last 2 ns between *Mt*CMPK and *Mt*CMPK-CMP is 9.02 Å demonstrating a large motion in this region. These data are is in agreement with RMSF, which thus confirms the differences between ligand-free enzyme and enzyme in complex with CMP.

The sulphate ion bound in the phosphate donor site

*Mt*CMPK contains the classical mononucleotide-binding motif: a β strand (β1 for *Mt*CMPK) followed by a helix (α1) connected by a glycine-rich loop with a strongly conserved fingerprint sequence Gly-X-X-Gly-X-Gly-Lys (P loop), where X stands for any amino acid [8]. This motif forms a giant anion hole also known as P-loop. In *Mt*CMPK, this motif corresponds to residues Gly13-X-X-Gly16-X-Gly18-Lys. The RMSF values indicate the high flexibility of helix α1 (Lys19-Leu30) and the phosphate donor site (Gly13-Gly18) in apo form. The presence of CMP causes a major stability and approximation of this structure when compared with its ligand-free model. It has been suggested that negatively charged ions with tetrahedral geometry (such as sulphate and phosphate ions) can inhibit kinases from binding nucleotides bearing a β-phosphate [39].

Interaction with cytidine-5′-monophosphate

The specificity and affinity between enzyme and its inhibitor depend on directional hydrogen bonds and ionic interactions, as well as on shape complementarity of the contact surfaces of both partners [40]. Analysis of the hydrogen bonds between cytidine-5′-monophosphate and *Mt*CMPK reveals ten intermolecular hydrogen bonds and 14 with *Ec*CMPK, the residues involved in the interaction with ligand are showed in Table 1. Analysis of the affinity constants between complex protein-ligand calculated by the program X-SCORE, SCORE and PERALS (Table 2) reveals that the pKd value of 4.93 calculated by SCORE program is more accurate as compared to the experimental value of 4.45 pKd units [41]. *Ec*CMPK has higher affinity for CMP than *Mt*CMPK, which is consistent with the larger number of hydrogen bonds for the latter as compared with the former.

Conclusions

The molecular models of *Mt*CMPK show that the interaction with CMP is favorable as observed for *Ec*CMPK. The results obtained are in agreement with experimental data [12] demonstrating that the LID domain, NMP_{bind} domain and phosphate donor site have low mobility when complexed with CMP and large motion in ligand-free form. Moreover, the data presented here suggest that the mode of action for *Mt*CMPK may be similar to *Mt*SK, with the open/closed conformational changes of the LID domain and the substrate binding loop involved in substrate entrance and exit.

Table 1 Intermolecular contacts of *Ec*CMPK and *Mt*CMPK with CMP

Residues/ligands	EcCMPK	Residues/ligands	MtCMPK
Met133	SD-N19 -> 3.67 Å	Arg133	NH2-O3 -> 3.01 Å
Arg41	NH2-O4 -> 3.50 Å		NE-N14 -> 3.13 Å
Arg181	NH1-O10 -> 2.96 Å		N-N19 -> 3.06 Å
Asp185	OD2-O10 -> 2.81 Å	Arg183	NE-O10 -> 2.99 Å
	OD1-O12 -> 2.63 Å	Asp187	OD2-O10 -> 2.85 Å
Arg110	NH1-O16 -> 2.73 Å		OD1-O12 -> 2.84 Å
	NH2-O16 -> 3.30 Å	Arg111	H2-O16 -> 3.09 Å
	NH2-N17 -> 3.14 Å	Arg190	NH1-O16 -> 2.96 Å
Arg188	NH1-O16 -> 2.87 Å		NH2-O16 -> 2.89 Å
	NH2-N17 -> 2.75 Å	Asp134	OD1-N19 -> 2.85 Å
Ser36	OG-N19 -> 2.82 Å		–
Arg131	N-N19 -> 3.05 Å		–
	NH2-O3 -> 3.48 Å		–
Asp132	OD1-N19 -> 3.16 Å		–
Total Number of Hydrogen Bonds	14		10

Table 2 pKds for *Ec*CMPK and *Mt*CMPK

	XSCORE	SCORE	PEARLS
*Ec*CMPK	6.31 (4.45)	4.93 (4.45)	6.03 (4.45)
*Mt*CMPK	5.96	4.69	5.14

In parentheses show the experimental value for *Ec*CMPK complexed with CMP [35]
The results were generated using XSCORE [16], SCORE [17] and PEARLS [18]

Acknowledgements This work was supported by grants from Millennium Institutes (CNPq-MCT) to DSS, LAB and WFA. WFA, LAB and DSS are research career awardees from the National Research Council of Brazil (CNPq).

References

1. World Health Organization (2005) World health organization report: global tuberculosis control - surveillance, planning, financing. Geneva, Switzerland
2. Dye C (2006) Lancet 367:938–940
3. Pablos-Mendez A, Gowda DK, Frieden T (2002) Bulletin of the World Health Organization 80(6):489–500
4. CDC (Centers for Disease Control and Prevention) (2006) Morb Mortal Wkly Rep 55:301–305
5. WHO: Report WHO/HTM/TB/2006.375, (2006) Geneva
6. Dorman SE, Chaisson RE (2007) Nature 113:295–298
7. Singh JA, Upshur R, Padayatchi N (2007) PLoS Medicine 4(1): 50
8. Leipe DD, Koonin EV, Aravind L (2003) J Mol Biol 333:781–815
9. Liou JY, Dutschman GE, Lam W, Jiang Z, Cheng YC (2002) Cancer research 62:1624–1631
10. Yu L, Mack J, Hajduck PJ, Kakavas SJ, Saiki AYC, Lerner CG, Olejniczak ET (2003) Protein Sci 12:2606–2621
11. Dhaliwal B, Ren J, Lockyer M, Charles I, Hawkins AR, Stammers DK (2006) Acta Crystallogr F 62:710–715
12. Briozzo P, Golinelli-Pimpaneau B, Gilles AM, Gaucher JF, Burlacu-Miron S, Sakamoto H, Janin J, Bârzu O (1998) Structure 6:1517–1527
13. Kroemer RT, Doughty SW, Robinson AJ, Richards WG (1996) Protein Eng 9(6):493–498
14. Sali A, Blundell TL (1993) J Mol Bio 234(3):779–815
15. Sali A, Overington JP (1994) Protein Sci 3(9):1582–1596
16. Canduri F, Uchoa HB, de Azevedo WF Jr, (2004) Biochem Biophys Res Commun 324(2):661–666
17. Hall TA (1999) Nucleic Acids Symp Ser 41:95–98
18. de Azevedo WF, Mueller-Dieckmann JH, Schulze-Gahmen U, Worland PJ, Sausville E, Kim SH (1996) Proc Natl Acad Sci USA 93:2735–2740
19. Wang R, Lai L, Wang S (2002) J Comput-Aided Molecular Des 16:11–26
20. Wang R, Liu L, Lai L, Tang Y (1998) J Mol Model 4:379–394
21. Han LY, Lin ZR, Zheng CJ, Cao ZW, Xie B, Chen YZ (2006) J Chem Inf Model 46:445–450
22. Laskowski RA, Macarthur MW, Moss DS, Thornton JM (1993) J Appl Crystallogr 26:283–291
23. Uchoa HB, Jorge GE, Da Silveira NJF, Camera JC, Canduri F, De Azevedo WF (2004) Biochem Biophys Res Comum 325:1481–1486 DOI 10.1016/j.bbrc.2004.10.192
24. van der Spoel D, Lindahl E, Hess B, Groenhof G, Mark AE, Berendsen HJC (2005) J Comp Chem 26 p. 1701–1718 http://www.gromacs.org
25. (a) van Aalten DMF, Bywater B, Findlay JBC, Hendlich M, Hooft RWW, Vriend GJ (1996) Comput Aided Mol Des 10, 255–262 (b) http://davapc1.bioch.dundee.ac.uk/programs/prodrg/prodrg.html
26. Schmidt MW, Baldridge KK, Boatz JA, Elbert ST, Gordon MS, Jensen JH, Koseki S, Matsunaga N, Nguyen KA, Su SJ, Windus TL, Dupuis M, Montgomery JA (1993) J Comput Chem 14: 1347–1363
27. Guex N, Peitsch MC (1997) Electrophoresis 18:2714–2723
28. Berendsen HJC, Postma JPM, van Gunsteren WF, Hermans J (1981) Interaction models for water in relation to protein hydration. In: Pullman B (ed) Intermolecular forces. Reidel, Dordrecht, The Netherlands, pp 331
29. Hess B, Bekker H, Berendsen HJC, Fraaije JGEM (1997) J Comput Chem 18:1463
30. Miyamoto S, Kollman PA (1992) J Comput Chem 13:952
31. Chowdhuri S, Tan ML, Ichiye T (2006) J Chem Phys 125:144513
32. Darden T, York D, Pedersen LA (1993) J Chem Phys 98: 10089–10092
33. Norberto de Souza O, Ornstein RL (1999) J Biomol Struct Dyn 16:1205–1218
34. Cole ST, Brosch R, Parkhill J, Garnier T, Churcher C, Harris D, Gordon SV, Eiglmeier K, Gas S, Barry CE, Tekaia F, Badcock K, Basham D, Brown D, Chillingworth T, Connor R, Davies R, Devlin K, Feltwell T, Gentles S, Hamlin N, Holroyd S, Hornsby T, Jagels K, Barrell BG (1998) Nature 393(1998):537–544
35. Gu Y, Reshetnikova L, Li Y, Wu Y, Yan H, Singh S, Ji S (2002) J Molec Biol 319:779–789
36. Stehle T, Schultz GE (1992) J Mol Biol 224:1127–1141
37. Pereira JH, Oliveira JS, Canduri F, Dias MVB, Palma MS, Basso LA, Santos DS, Azevedo Jr WF (2004) Acta Cryst D 60:2310–2319
38. Jencks WP (1975) Adv Enzymol Relat Areas Mol Biol 43: 219–410
39. Gan J, Gu Y, Li Y, Yan H, Ji X (2006) Biochemistry 45:8539–8545
40. de Azevedo WF, Canduri F, Fadel V, Teodoro LG, Hial V, Gomes RA (2001) Biochem Biophys Res Commun 287(1):277–281
41. Schomburg I, Chang A, Ebeling C, Gremse M, Heldt C, Huhn G, Schomburg D (2004) Nucleic Acids Res Jan 1:32, Database issue: D431–3